PERGAMON

Journal of Structural Geology 23 (2001) 33–44

JOURNAL OF STRUCTURAL GEOLOGY

www.elsevier.nl/locate/jstrugeo

A laser-probe $^{40}Ar/^{39}Ar$ study of pseudotachylite from the Tambach Fault Zone, Kenya: direct isotopic dating of brittle faults

S.C. Sherlock[a,1,*], R. Hetzel[b]

[a]*Department of Earth Sciences, The Open University, Milton Keynes, MK7 6AA, UK*
[b]*GeoForschungsZentrum (GFZ) Potsdam, Telegrafenberg, 14473 Potsdam, Germany*

Received 29 March 2000; accepted 19 June 2000

Abstract

Understanding the tectonic evolution of orogenic belts and intracratonic areas depends on our ability to determine the age of tectonic features on a variety of scales. This study demonstrates the value of the laser-probe $^{40}Ar/^{39}Ar$ dating technique, which, if applied to fault-derived pseudotachylites, may be used to directly determine the age of brittle faults. The laser-probe technique affords high spatial resolution, enabling a greater opportunity for discriminating between pseudotachylite matrix, host-rock clasts and alteration products that are often present in varying proportions within pseudotachylites. The laser-probe $^{40}Ar/^{39}Ar$ technique has been applied to pseudotachylite samples from the Tambach Fault Zone (TFZ), a major NW–SE trending strike-slip fault within the Kenyan part of the Late Proterozoic/Early Palaeozoic Mozambique Belt. The pseudotachylites of the TFZ were previously thought to have formed either (i) at about 530–430 Ma, or (ii) during the Cenozoic evolution of the Kenya Rift. In the latter case, seismic slip on the rift-bounding normal fault would have generated the pseudotachylites, due to the reactivation of old NW–SE trending structures in the basement. Based on our new data, we interpret the pseudotachylite formation age to be 400 Ma. This rules out the possibility that the pseudotachylites are related to the formation of the Kenya Rift. Although the inherited basement faults may have been locally reactivated as transfer faults, reactivation of these structures during rifting did not occur beyond the margins of the Kenya Rift.

1. Introduction

Our understanding of the tectonic evolution of either orogenic belts or intracratonic areas is dependent on our ability to obtain and understand isotopic age determinations of ductile shear zones and brittle faults on a range of crustal scales. The age of ductile shear zones that were active at mid- to lower-crustal levels may be directly determined from mylonitic rocks by isotopic dating of syn-tectonic minerals such as mica (e.g., Inger et al., 1996; Reddy et al., 1996; Freeman et al., 1997), sphene (Resor et al., 1996), or monazite (e.g., Schärer et al., 1994). The direct isotopic dating of brittle faults in the upper crust is problematic due to the generally fine-grained nature of the fault-derived material and the low temperatures associated with upper-crustal faulting. Although there has been some success in dating clay-rich fault gouges using K–Ar (Kralik et al., 1987), the technique has not yet been widely adopted. Ages of brittle faults are, therefore, most commonly constrained indirectly by stratigraphic consideration, or by the application of isotopic methods to syn- or post-tectonic volcanic rocks, or, most recently, feldspar thermochronology on clasts within breccias (Dunlap and Fossen, 1998; Eide et al., 1997). In areas with crystalline basement, where any sedimentary or volcanic stratigraphic markers are lacking, it is extremely difficult to determine the age of brittle faults. Differential vertical movements of crustal blocks may be resolved by fission-track thermochronology, if the vertical displacement on faults exceeds a few hundred metres (Foster and Gleadow, 1996). However, the timing of faulting that results in either smaller displacements or strike-slip motion, would remain undetected since the apparent fission track ages would be the same on both sides of the fault.

The isotopic dating of pseudotachylites offers a unique way to directly obtain geochronological information from brittle fault rocks. Pseudotachylite refers to dark aphanitic veins, composed of friction-derived melt material interspersed with clasts and crystals from the host-rock, and is thought to be formed in response to either rapid tectonic faulting, meteorite impacts, or landslides (e.g. Magloughlin

* Corresponding author.
E-mail address: s.sherlock@open.ac.uk (S.C. Sherlock).
[1] Current address: The Geological Survey of Norway, Leiv Eirikssons vei 39, 7491 Trondheim, Norway

0191-8141/01/$ - see front matter
PII: S0191-8141(00)00082-1

and Spray, 1992; Reimold, 1995; Reimold, 1998). Tectonic pseudotachylites commonly have sharp boundaries and show a clear association with fault zones (Magloughlin and Spray, 1992). By virtue of their nature, pseudotachylites are considered an ideal target material when attempting to directly date fault movements. In addition, the often high potassium content of the melt material makes pseudotachylite an ideal candidate for $^{40}Ar/^{39}Ar$ dating. Pseudotachylites have been described from many large-scale fault zones, for example the Alpine Fault (Bossière, 1991), the Outer Hebrides Thrust (e.g., Maddock et al., 1987), and the Periadriatic Fault System (Müller, 1997). The number of fault-related pseudotachylite occurrences reported in the literature is steadily increasing (Lin, 1994; McNulty, 1995; Hetzel et al., 1996; Karson et al., 1998). Dating pseudotachylites using bulk K–Ar and $^{40}Ar/^{39}Ar$ techniques has proved difficult (e.g., Reimold et al., 1990, 1992; Spray et al., 1995; Müller, 1997) due to the highly heterogeneous nature of pseudotachylites and the fact that faults may often have multi-episodic histories. However, the development of the laser probe $^{40}Ar/^{39}Ar$ technique (e.g., McConville et al., 1989) has enabled the successful dating of some pseudotachylites (Kelley et al., 1994; Spray et al., 1995; Karson et al., 1998).

This contribution describes a laser-probe $^{40}Ar/^{39}Ar$ study of pseudotachylite from a major strike-slip fault in the crystalline basement of western Kenya. The results underline the great potential of using pseudotachylites to determine the age of brittle faults. We also discuss the assumptions that have to be made about argon behaviour in pseudotachylite and demonstrate the complexity of dating such heterogeneous material.

2. Formation mechanism of pseudotachylites and the processes controlling their argon systematics

Tectonic pseudotachylites form during seismic events by cataclastic grain size reduction followed by friction-induced melting (Spray, 1992; Spray et al., 1995; Magloughlin and Spray, 1992; Hetzel et al., 1996). It is this second criterion that is important in distinguishing pseudotachylites from even the finest grained cataclasites, for which the $^{40}Ar/^{39}Ar$ technique is unsuited unless there is a potassium-bearing neo-crystalline mineral growth such as white mica or illite. Markedly planar fault veins, where the melt has been generated, can be distinguished from smaller, irregular injection veins where the pseudotachylite material was injected into tension fractures (Sibson, 1975). Elongate, small (i.e. <40 μm) crystals of minerals such as plagioclase, amphibole, or biotite may grow as randomly-oriented 'microlites' in the friction melt. Hydrous ferromagnesian host-rock minerals such as mica and/or amphibole are essential components in the formation of frictional melt, mainly due to their low fracture toughness, low shear yield strength, and low melting points (Spray, 1992). In addition, pseudotachylites may contain significant amounts of potassium derived from the host-rock micas and/or amphiboles (e.g., Spray, 1993), and are, therefore, suitable candidates for $^{40}Ar/^{39}Ar$ geochronology.

In general terms, the successful dating of pseudotachylites requires that a number of criteria are met: a) argon must be able to outgas from the melt during rapid melting and cooling associated with pseudotachylite formation, b) the analysis of host-rock porphyroclasts containing inherited argon must be avoided, c) the argon system must not be disturbed by subsequent thermal events or pervasive fluid fluxes, and d) argon loss by volume diffusion after the pseudotachylite-forming event has to be minimal. These four assumptions can be broadly categorised and discussed in terms of those processes which facilitate the outgassing of argon, and those processes that prevent the outgassing of argon, from both the fine-grained pseudotachylite matrix and inherited host-rock clasts.

2.1. Argon loss from the melt

The effective removal of inherited radiogenic argon from the melt forms the basis for the application of the $^{40}Ar/^{39}Ar$ technique to pseudotachylite. It also precludes the extension of this technique to cataclasites, which, by definition, do not contain a melt fraction and will, therefore, not have experienced effective degassing of radiogenic argon, inherited from the precursor rock.

From the few studies that attempted to constrain the temperature of pseudotachylite formation, friction melt is believed to form at high temperatures, generally in excess of 1000°C (e.g., Lin, 1994; Hetzel et al., 1996, and references therein). Pseudotachylite that formed in broadly granitic host-rocks, such as those in the TFZ, contains 40 to 60 wt% SiO_2, (e.g., Bossière, 1991; Magloughlin and Spray, 1992; Spray, 1993). In more silicic host-rocks this may increase, for example >75 wt% SiO_2 has been reported for pseudotachylites hosted by Si-rich lavas in the Witwatersrand Basin (Killick et al. 1988; Reimold et al., 1999). The high formation temperatures and the low viscosity of the melt, which has been described as being similar to basaltic magmas at the same temperature (e.g., Spray, 1993) should facilitate the outgassing of argon from the melt. As the solubility of argon in silicate melts decreases linearly with decreasing pressure (White et al., 1989; Carroll and Stolper, 1993), the sudden pressure decrease associated with the failure of the country rock and the formation of injection veins should enable argon to leave the melt.

2.2. Argon retention in the melt

The relatively high solubility of argon in silicate melts (White et al., 1989; Draper and Carroll, 1995) may prevent complete argon loss from the melt during pseudotachylite formation. In consequence, it cannot be assumed that all argon will escape from the pseudotachylite melt. Nevertheless, in this study, the relatively low SiO_2 content of ~55%

of the TFZ pseudotachylites (Hetzel et al., 1996) does not favour a high argon content in the melt, since the solubility of argon strongly decreases with decreasing SiO_2 (Carroll and Stolper, 1993; Shibata et al., 1998). The possible problem of Ar-retention by highly silicic melts diminishes with increasing K-content. As the studied pseudotachylites from the TFZ are very potassic (2.0 to 3.5 wt% K_2O), the radiogenic argon produced in situ following pseudotachylite formation is rather high and may mask any retained Ar. Precursor-rock clasts located within the fine-grained matrix are a further source of argon trapped, or 'inherited', during pseudotachylite formation, and should be avoided during $^{40}Ar/^{39}Ar$ analysis.

2.3. Post-crystallisation argon loss

The successful determination of a pseudotachylite age also depends on the prerequisite that the argon system has not been disturbed since melt formation due to either a subsequent metamorphic event, pervasive influx of fluids and/or alteration. The former may cause partial or complete resetting of the argon isotope system. Alteration products may lose radiogenic argon at low temperatures and, therefore, may yield younger, or mixed, ages and result in disturbed incremental step-heating spectra (e.g. Trieloff et al., 1994). By carefully investigating thin sections under the optical microscope and SEM, however, it is possible to identify areas that have suffered from alteration. These are generally characterised by fine-grained chloritisation of any biotite or amphibole host-rock clasts, sericitisation of feldspar clasts, and infilling of fractures with chlorite or sericite and possibly epidote (Trieloff et al., 1994). Argon loss might also occur by diffusion following pseudotachylite formation. This is less straightforward to identify than disturbance to the system by alteration, as there are no diagnostic optical properties that may be identified. Preliminary model calculations suggest that argon loss by diffusion following pseudotachylite formation will be negligible at temperatures below 150°C (Reimold et al., 1990), and according to their calculations a pseudotachylite that remains at 300°C for 0.1 Ma may lose 90% of its argon. Impact-related pseudotachylites from Sudbury yielded ages ranging from 1850 to 1000 Ma, with some samples yielding multiple ages that do not correlate to known geological events (Thompson et al., 1998). Argon diffusion modelling indicates that subsequent to pseudotachylite formation at approximately 1850 Ma, the impact structure was buried to depths of 5 to 6 km, and temperatures of 160 to 180°C were maintained until exhumation at 1000 Ma (Thompson et al., 1998). The TFZ pseudotachylites were formed at depths of approximately 3 to 4 km, and temperatures of up to 150°C, with no further burial subsequent to pseudotachylite formation, and thus argon loss by volume diffusion is unlikely to have played any significant part in their argon isotopic system.

2.4. Excess argon gain

Excess argon might affect the argon systematics of the pseudotachylite. Excess argon is a component of ^{40}Ar additional to both radiogenic and atmospheric ^{40}Ar, which, if present, will result in ages older than the true age of the pseudotachylite, by artificially increasing the $^{40}Ar/^{39}Ar$ ratio. This is a commonly reported problem in dating high-pressure/low-temperature metamorphic rocks and minerals (Arnaud and Kelley, 1995; Ruffét et al., 1997; Scaillet, 1996; Sherlock and Arnaud, 1999; Sherlock et al., 1999). The excess ^{40}Ar will mix with K-derived radiogenic ^{40}Ar and any trapped atmospheric ^{40}Ar in the pseudotachylite, resulting in an elevated $^{40}Ar/^{39}Ar$ ratio and an anomalously old apparent age. It is impossible, however, to distinguish between any 'inherited' ^{40}Ar, derived from the precursor-rock minerals and unable to escape the melt during pseudotachylite formation and crystallisation, and excess ^{40}Ar which has been introduced into the pseudotachylite at a later stage, for example during alteration. The only way in which to attempt to differentiate between ^{40}Ar unable to escape from the melt and excess argon that arrived with late fluids is to investigate the absence or presence of alteration products.

3. Geological setting

3.1. Mozambique Belt

Basement rocks in Kenya mainly comprise igneous and high-grade metamorphic rocks of the Late Proterozoic/Early Palaeozoic Mozambique Belt (Shackleton, 1986; Key et al., 1989). The N–S-trending Mozambique Belt is interpreted to have formed during continent–continent collision between East and West Gondwana (Burke and Sengör, 1986; Shackleton, 1986). Petrological and geochronological investigations suggest a prolonged tectonometamorphic evolution for the Mozambique Belt, following a cooling path from granulite to amphibolite and, then, greenschist facies, with three major stages identified between ~850 and ~430 Ma (Maboko et al., 1985; Charsley, 1987; Key et al., 1989, and references therein). An early syn-collisional phase of SW- to W-directed thrusting occurred under granulite facies, at ~850–720 Ma (Rb–Sr whole rock and Sm–Nd garnet; Key et al., 1989; Smith and Mosley, 1993). This was followed by a phase of sinistral orogen-parallel shearing under retrograde amphibolite facies conditions, at ~635–550 Ma (Rb–Sr whole rock and K–Ar biotite; Key et al., 1989). End-collisional events at ~530–430 Ma (Rb–Sr whole rock and K–Ar biotite; Maboko et al., 1985; Key et al., 1989) were dominated by ductile/brittle faulting along NW–SE trending shear zones and faults, of which the TFZ is one. These prominent NW–SE-trending structures are characterised by extensive brecciation, cataclastic deformation, and pseudotachylite zones (Smith and Mosley, 1993; Key et al., 1989; Charsley, 1987).

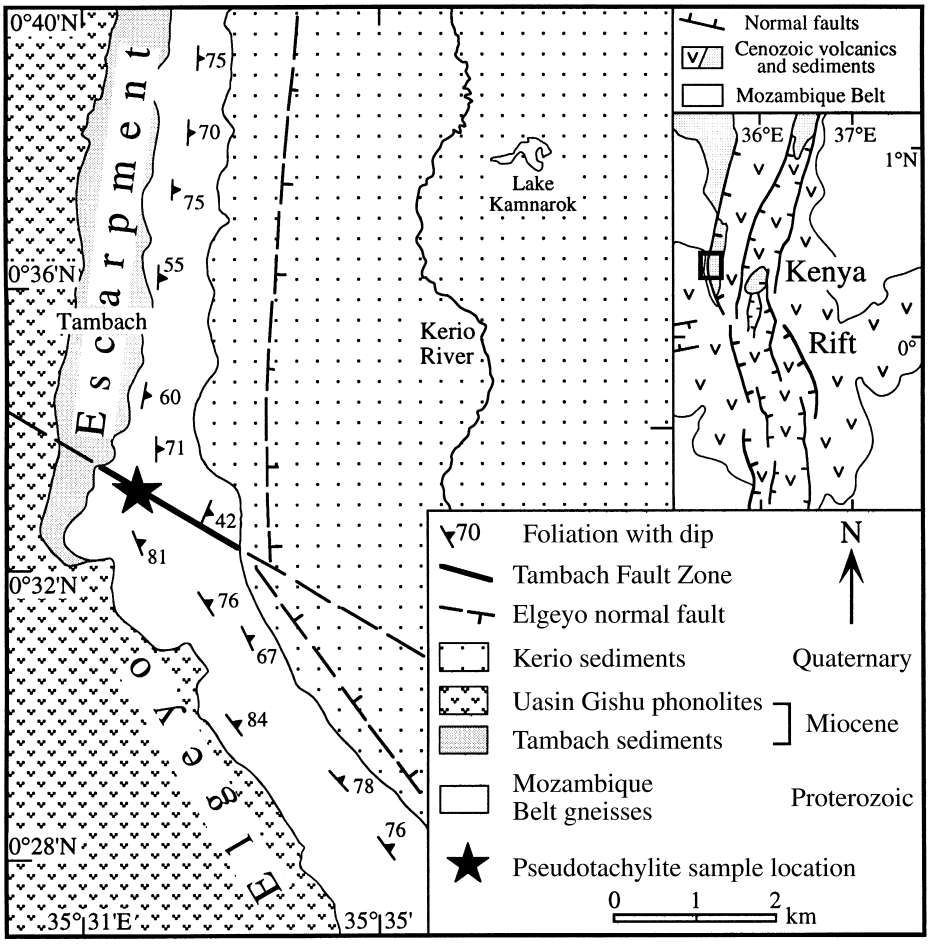

Fig. 1. Simplified geological map of the southern Elgeyo Escarpment showing the location of the Tambach Fault Zone. Inset in upper right corner shows the location within the Kenya Rift.

3.2. Pseudotachylite sample location and cooling history of its host rock

The Tambach Fault Zone (TFZ) transects the Mozambique Belt basement at the Elgeyo Escarpment (Fig. 1), which is the western border of the northern Kenya Rift and the expression of the rift-bounding Elgeyo normal fault (Mugisha et al., 1997). Two main types of gneiss occur in the TFZ. Biotite-bearing quartz-feldspar gneiss is the dominant rock type but it contains a minor component of hornblende-gneiss. The pseudotachylite-bearing TFZ is well-exposed 2 km south of Tambach village along the main road between Kabarnet and Eldoret. The subvertical NW–SE-trending pseudotachylite fault veins crosscut the E to SE-dipping foliation of the gneisses at a high angle. Pseudotachylite samples were collected along the main road at an altitude of ~1700 metres, 100 to 700 m WNW of a prominent tourist view-point (0°33.6'N and 35°31.8'E, Fig. 1).

Metamorphic parageneses and textures that occur in mafic boudins within the gneisses at the Elgeyo Escarpment are indicative of isothermal decompression during granulite-facies metamorphic conditions (Hetzel and Strecker, 1994). The main foliation observed in the gneisses along the Elgeyo Escarpment (Fig. 1) was generated in a sinistral ductile shear zone during retrograde amphibolite-facies conditions, as indicated by the syndeformational growth of biotite and the growth of hornblende at the expense of pyroxene (Hetzel and Strecker, 1994). After this phase of ductile deformation, the temperature was still high enough to cause a pronounced static annealing, as indicated by straight equilibrium grain boundaries of quartz and the absence of undulose extinction. Cooling to subgreenschist-facies metamorphic conditions is recorded by the localised sericitisation of feldspars commonly observed adjacent to late-stage faults (Hetzel and Strecker, 1994). There is no evidence of any heating events post-dating this diaphtoritic alteration. The latest cooling history of the basement at the Elgeyo Escarpment is constrained by apatite fission track data which document that the base of a Cretaceous apatite partial annealing zone is at an elevation of 2.1 km, 60 km to the north of the TFZ (Foster and Gleadow, 1996). During the Late Cretaceous, a cooling/erosion event led to the cooling of the basement to $<60^{\circ}C$

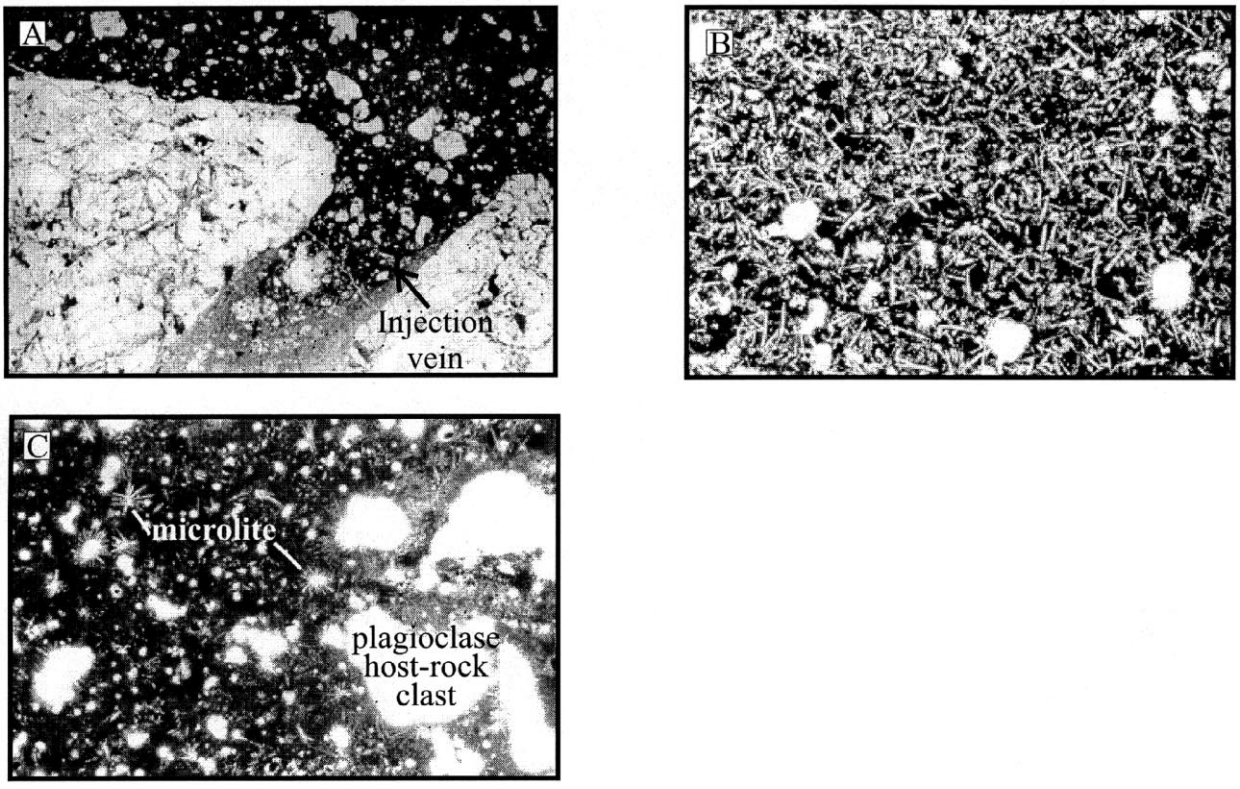

Fig. 2. Photomicrographs of Tambach Fault Zone pseudotachylite samples (see Fig. 1 for location), all taken in plane polarised light: (a) Contact between pseudotachylite fault vein (sample Ke3, avoided due to excessive host-rock clasts and alteration) and country rock gneiss, oriented subparallel to the long side of the photomicrograph. An injection vein is branching off from the fault vein at an angle of 50°. The long side of the photomicrograph is 5 mm. (b) Abundant feldspar microlites and a few host-rock porphyroclasts in pseudotachylite sample Ke5. The long side of the photomicrograph is 0.8 mm. (c) Radiating plagioclase microlites (< 20 μm) nucleated on plagioclase porphyroclasts.

(Foster and Gleadow, 1996). There is no petrological evidence in the host-rock gneisses for any overprinting thermal events, subsequent to faulting and pseudotachylite formation.

3.3. Kenya Rift

During the evolution of the Cenozoic Kenya Rift, the crustal-scale NW–SE-trending strike-slip faults of the Mozambique Belt have probably been reactivated as transfer faults (Smith and Mosley, 1993). The abrupt change in the trend of the northern Kenya Rift at 0°32'N occurs exactly at the intersection of the TFZ with the Elgeyo normal fault (Fig. 1 inset map). Thus, the TFZ may have acted as a transfer fault that linked different segments of the rift-bounding Elgeyo normal fault (Hetzel and Strecker, 1994). Smith and Mosley (1993) have speculated that the Tambach pseudotachylites are Cenozoic in age and may indicate that seismic slip on the Elgeyo normal fault was in part accommodated along NW–SE-trending structures in the basement. Alternatively, Hetzel and Strecker (1994) related the pseudotachylytes to the late-orogenic evolution of the Mozambique Belt and emphasised that the TFZ was not reactivated *beyond* the rift margin. Age dating of the pseudotachylites is thus critical for distinguishing between these two different models for the reactivation of inherited NW–SE-trending faults in the Mozambique Belt basement.

4. Pseudotachylite description

The TFZ pseudotachylites display a reddish/brown to black matrix, and on the mm-scale contain 10–25% porphyroclasts that are mainly quartz and subordinate feldspar that range from 30 μm to 1 mm in diameter (Fig. 2). The pseudotachylite matrix is free of biotite, hornblende and pyroxene porphyroclasts, which only occur as parts of host-rock lithoclasts. Commonly the pseudotachylite fault veins show a distinct microstructure, which is characterised by a marginal cataclasite domain of up to 200 μm thick, and a microlitic domain in the centre of the veins. The marginal cataclasite zone adjacent to the host-rock is almost continuous along the vein margins and is characterised by a matrix of fine-grained rock fragments and porphyroclasts of grain sizes <2 μm. The central microlitic domain has abundant plagioclase and hornblende microlites, variable amounts of quartz porphyroclasts and subordinate amounts of feldspar porphyroclasts that often form nuclei for radially-arranged plagioclase microlites (Fig. 2b, c).

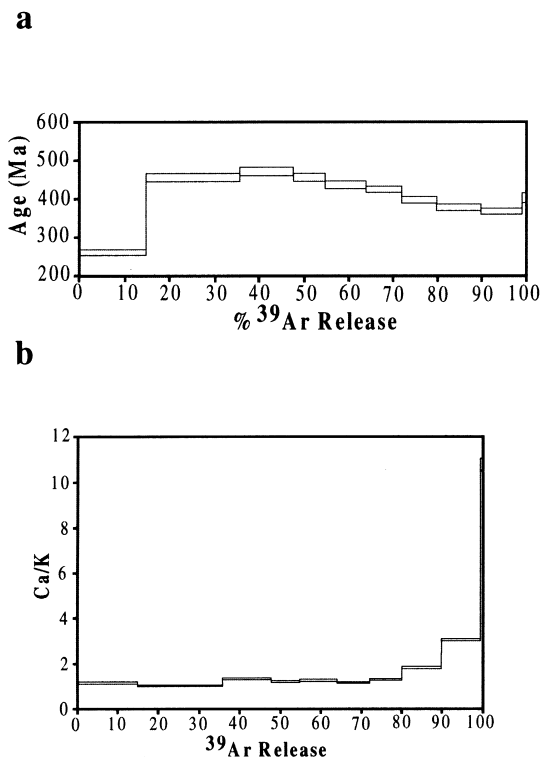

Fig. 3. (a) Bulk step-heating release spectrum for sample P37. No plateau age could be determined, the total gas age is 405 ± 8 Ma. (b) Ca/K ratio plot corresponding to the step-heating release spectrum for sample P37.

Fourteen pseudotachylite samples hosted by the quartz-feldspar gneiss were collected from the TFZ. Samples Ke1, Ke4, Ke5, Ke9 and P37 were selected for laser-probe $^{40}Ar/^{39}Ar$ analysis, as they have the lowest abundances of host-rock clasts. P37 (sample A of Hetzel et al., 1996) was chosen, as previously obtained $^{40}Ar/^{39}Ar$ incremental-heating spectrum serves as a direct comparison of a bulk sampling technique versus the infrared laser-probe extraction technique. Sample P37 has also been chemically characterised (sample A, Hetzel et al., 1996). Sections chosen for irradiation were located as far as possible from the nearest host-rock contact to avoid the high inherited argon component associated with the host-rocks of pseudotachylites (Kelley et al., 1994).

5. Experimental methods

To determine the age of the pseudotachylite matrix, laser spots of approximately 50 μm in diameter were positioned to avoid quartz and feldspar clasts, regions dominated by microlites, and the outer cataclasite-rich regions of the pseudotachylites. Where possible, analyses were also made of quartz and feldspar clasts to compare with results from matrix pseudotachylite. For infrared laser spot analysis, the samples were prepared by cutting 300-μm-thick sections, polished on one side and ultrasonically cleaned alternately in methanol and de-ionised water. Pieces of pseudotachylite, approximately 5 × 5 mm in size, were wrapped in aluminium foil and irradiated at the Risø National Laboratory, Denmark. The GA1550 biotite standard, with an age of 98.79 ± 0.96 Ma (Renne et al., 1998), was used to monitor the fast-neutron flux; the calculated *J* value is 0.0064 ± 0.000032. The samples were analysed at The Open University (UK) using a focused CW Nd-Yag infrared laser with an external shutter; the extracted argon isotopes ^{35}Ar to ^{41}Ar were measured in a MAP 215-50 noble gas mass spectrometer. Analyses were corrected for blanks, ^{37}Ar decay and neutron-induced interference reactions using the correction factors: $(^{39}Ar/^{37}Ar)_{Ca} = 0.00067$, $(^{36}Ar/^{37}Ar)_{Ca} = 0.000255$ and $(^{40}Ar/^{39}Ar)_{K} = 0.048$. For the incrementally heated sample, P37, the pseudotachylite was crushed and sieved, and black matrix particles were hand-picked from the 250 to 500 μm size fraction in an attempt to avoid quartz and feldspar clasts. The sample was irradiated in the FRG1 reactor at the Nuclear Research Centre at Geesthacht (Germany) with the biotite neutron flux monitor HD-B1 (24 Ma, Lippolt and Hess, 1988). Samples were incrementally heated using a resistance furnace, and argon isotopes measured in a MAT GD-150 mass spectrometer at the Max-Planck Institut für Chemie in Mainz, Germany. All calculated ages are reported with 2σ errors, intra-laboratory uncertainties (1.5 to 2%) have been calculated by statistical propagation of uncertainties associated with each isotopic ratio, correction factors and *J* value.

6. Results

Data for all samples are presented in Table 1. Laser spot ages for the pseudotachylite matrix for all five samples range from 858 ± 9 Ma to 313 ± 15 Ma. Given the heterogeneity of the pseudotachylite material, even with an analytical resolution of 50 μm, this represents a large range of ages. As a broadly comparative measure, mean ages for each sample have been calculated, and are in the range 396 ± 10 Ma to 507 ± 192 Ma (Table 2). Sample Ke1 has the widest range of matrix ages, from 313 ± 15 Ma to 858 ± 9; the mean ages of the other samples form a narrow range, from 396 ± 10 Ma to 414 ± 15 Ma. For sample P37, the laser spot ages are 377 ± 7 to 411 ± 10 Ma, with a mean age of 396 ± 10 Ma. The incremental-heating spectrum for sample P37 (Fig. 3a) does not adhere to the generally accepted criteria for a plateau age, namely, at least, three concordant steps representing a significant proportion of the total ^{39}Ar released (e.g., Dalrymple and Lanphere, 1974; Lanphere and Dalrymple, 1978; Berger and York, 1981), which for most workers is approximately 50%. However, the ages for individual steps are in the range 260 ± 6 Ma to 471 ± 10 Ma, with a total gas age of 405 ± 8 Ma, which is within error of the mean laser spot age of 396 ± 10 Ma. The quartz and feldspar clasts which were analysed in samples Ke1 and Ke5 gave apparent ages of 365 ± 7 Ma and

Table 1
Argon isotope and age data for the five pseudotachylite samples.

Sample	$^{36}Ar/^{39}Ar$	$^{37}Ar/^{39}Ar$	$^{38}Ar/^{39}Ar$	$^{40}Ar/^{39}Ar$	$^{*40}Ar/^{39}Ar$	Age	± (2σ)
Ke1 matrix	0.003533	0.156475	0.035074	91.01878	89.974742	820	6
Ke1 matrix	0.01499	0.146512	0.023594	40.78876	36.359134	377	4
Ke1 matrix	0.003107	0.156775	0.037065	71.05009	70.13199	669	18
Ke1 matrix	0.014323	0.200586	0.019943	39.91432	35.681964	371	23
Ke1 matrix	0.036478	0.19807	0.026869	46.52616	35.747054	372	17
Ke1 matrix	0.020185	0.101926	0.020851	38.49198	32.527387	341	18
Ke1 matrix	0.005376	0.149985	0.029991	52.17231	50.583621	506	7
Ke1 matrix	0.001526	0.177227	0.036431	95.62543	95.174605	858	9
Ke1 matrix	0.020283	0.139929	0.017377	35.64504	29.651304	313	15
Ke1 matrix	0.004117	0.099591	0.027887	44.83871	43.622086	444	12
Ke1 quartz clast	0.012743	0.143357	0.02466	38.79269	35.027032	365	7
Ke1 quartz clast	0.014528	0.164187	0.046319	56.92164	52.628483	524	32
Ke4 matrix	0.019139	0.181189	0.02936	39.62322	33.967605	355	11
Ke4 matrix	0.027046	0.09713	0.035528	40.90027	32.908251	345	44
Ke4 matrix	0.023636	0.187339	0.03795	52.55464	45.570077	462	62
Ke4 matrix	0.021249	0.207286	0.045676	49.82136	43.542267	443	21
Ke4 matrix	0.020115	0.14323	0.037627	44.13631	38.192374	395	16
Ke4 matrix	0.02407	0.168459	0.042844	45.02638	37.913563	392	13
Ke4 matrix	0.019527	0.176859	0.031833	41.01563	35.245373	367	10
Ke4 matrix	0.017364	0.173793	0.033093	44.52074	39.389806	406	17
Ke4 matrix	0.016246	0.168738	0.028237	49.42585	44.625179	453	16
Ke4 matrix	0.018693	0.138315	0.027348	39.49678	33.973069	355	8
Ke4 matrix	0.018198	0.175311	0.029816	41.81852	36.441061	378	14
Ke4 matrix	0.012038	0.177865	0.032505	43.31743	39.7602	409	6
Ke5 matrix	0.019226	0.160624	0.034591	47.26619	41.58477	426	21
Ke5 matrix	0.014446	0.135868	0.02945	46.50641	42.237492	432	13
Ke5 matrix	0.01415	0.186186	0.038064	46.30011	42.118882	431	15
Ke5 matrix	0.015989	0.157381	0.030073	46.0971	41.372371	424	8
Ke5 matrix	0.024979	0.153261	0.032542	46.37095	38.98952	402	11
Ke5 matrix	0.023547	0.205523	0.041432	46.95411	39.995853	411	8
Ke5 matrix	0.022563	0.135626	0.030605	46.76727	40.099914	412	4
Ke5 matrix	0.018972	0.155062	0.042029	45.86124	40.254916	414	8
Ke5 matrix	0.021698	0.180882	0.031444	47.1352	40.72345	418	11
Ke5 matrix	0.016723	0.214815	0.038014	45.38424	40.442532	415	8
Ke5 matrix	0.018235	0.185518	0.032421	45.65125	40.262677	414	9
Ke5 feldspar clast	0.026102	0.436326	0.057851	41.85632	34.143033	357	63
Ke5 quartz clast	0.014384	0.125355	0.03239	45.8187	41.568202	426	12
Ke9 matrix	0.009455	0.282772	0.034662	39.18114	36.387122	378	15
Ke9 matrix	0.003454	0.211793	0.052592	44.65681	43.63606	444	7
Ke9 matrix	0	0.209735	0.0526	37.99508	42.78084	437	87
Ke9 matrix	0.080664	0.299601	0.057673	64.62571	40.78937	418	29
Ke9 matrix	0.011328	0.249645	0.046205	41.43938	38.091863	394	12
Ke9 matrix	0.020574	0.250098	0.039451	44.79587	38.716162	399	5
Ke9 matrix	0.008038	0.228428	0.034549	43.01659	40.641459	417	4
Ke9 matrix	0.007144	0.200834	0.032229	38.86659	36.755609	381	14
Ke9 matrix	0.010743	0.250233	0.041956	41.6949	38.520349	398	5
Ke9 matrix	0.036533	0.235827	0.043693	48.22175	37.426164	387	7
Ke9 matrix	0.058526	0.229086	0.046607	54.71713	37.422609	387	6
P37 matrix (laser)	0.024802	0.214681	0.045217	46.88788	39.558904	407	13
P37 matrix (laser)	0.02892	0.206544	0.033591	44.82859	36.28275	377	11
P37 matrix (laser)	0.034749	0.221556	0.048027	48.30559	38.037325	393	4
P37 matrix (laser)	0.033074	0.227842	0.058524	49.03245	39.259121	404	12
P37 matrix (laser)	0.041476	0.219538	0.044333	49.13334	36.877154	382	14
P37 matrix (laser)	0.036593	0.218761	0.048023	49.44975	38.636545	399	6
P37 matrix (laser)	0.032738	0.298713	0.055437	49.53475	39.860672	410	12
P37 matrix (laser)	0.031326	0.249882	0.041746	45.56115	36.304219	377	7
P37 matrix (laser)	0.036506	0.250633	0.050449	49.54471	38.757292	400	9

Table 2
Intra-sample age ranges and mean ages for pseudotachylite matrix material from all five samples. The most erratic sample, Ke1, is highlighted in bold.

Sample	Age range	Mean age
Ke1	**313 ± 15 to 820 ± 6 Ma**	**507 ± 192 Ma**
Ke4	345 ± 44 to 462 ± 62 Ma	397 ± 20 Ma
Ke5	402 ± 11 to 432 ± 13 Ma	414 ± 15 Ma
Ke9	378 ± 15 to 444 ± 7 Ma	406 ± 17 Ma
P37 laser	377 ± 7 to 411 ± 10 Ma	396 ± 10 Ma
P37 furnace	Total gas age: 405 ± 8 Ma	05 ± 8 Ma

524 ± 32 Ma (both quartz, sample Ke1) and 357 ± 63 Ma and 426 ± 12 Ma (feldspar and quartz, respectively, sample Ke5) (Table 1).

The inverse isochron correlation diagram is used to determine whether the argon composition of the sample adheres to an atmospheric $^{40}Ar/^{36}Ar$ ratio (e.g., Dalrymple and Lanphere, 1974; Lanphere and Dalrymple, 1978; Berger and York, 1981; Heizler and Harrison, 1988). Any deviation from this ratio, which has a value of 295.5 (Steiger and Jäger, 1977), can be attributed to contamination by an ^{40}Ar component, such as excess argon, that is neither atmospheric nor derived from the decay of the K which is situated within the friction melt at the time of crystallisation. Fig. 4 is the inverse isochron correlation plot for sample Ke9, the only sample of the five analysed from the TFZ that contained sufficient ^{36}Ar to form a mixing line. A best-fit line intercepts the Y-axis within error of 295.5 and yields an intercept age of 401 ± 3 Ma. An intercept on the Y-axis that is within error of the value for atmospheric argon indicates that excess ^{40}Ar is not present.

Plotting both $^{37}Ar/^{39}Ar$ and $^{38}Ar/^{39}Ar$ reveals chemical information of the material ablated. ^{37}Ar is derived from the fast-neutron bombardment of calcium during sample irradiation, and ^{38}Ar is derived from chlorine during the same process. ^{37}Ar and ^{38}Ar, therefore, act as proxies for calcium and chlorine contents of the ablated material. In samples Ke1, Ke5 and Ke9 there is no correlation when $^{37}Ar/^{39}Ar$ is plotted against age. For samples Ke4 and P37 (laser spots) a good correlation exists, such that the oldest ages correspond to the highest $^{37}Ar/^{39}Ar$ ratios, and, therefore, the highest Ca/K ratios (Fig. 5a, b). In the incremental-heating spectrum of sample P37 (Fig. 3b), the highest temperature steps correspond to the highest $^{37}Ar/^{39}Ar$ ratios, though at 440 Ma this step is not the oldest. Similarly when $^{38}Ar/^{39}Ar$ is plotted against age, there is a broad correlation for samples Ke1 and P37 (Fig. 6a, b), with the oldest ages corresponding to the highest $^{38}Ar/^{39}Ar$ ratios, equivalent to the highest Cl/K ratios. Samples Ke4, Ke5 and Ke9 show no correlation of $^{38}Ar/^{39}Ar$ ratio with age. Analyses from quartz clasts in samples Ke1 and Ke5 fall into the $^{37}Ar/^{39}Ar$ and $^{38}Ar/^{39}Ar$ ranges for the matrix pseudotachylite material.

7. Discussion

7.1. Pseudotachylite formation age

Based on the following arguments we suggest that the TFZ pseudotachylite formation age is ~400 Ma. First, sample Ke5 has the narrowest age range (402 ± 11 to 432 ± 13 Ma) and a mean age of 414 ± 13 Ma. The piece chosen for irradiation from sample Ke5 contained less quartz and feldspar clasts than the other four samples, which is reflected by the lack of high Ca/K or Cl/K ratios. Second, a ~400 Ma formation age comes from Fig. 4, the inverse isochron correlation diagram for sample Ke9, suggesting that any contamination by excess ^{40}Ar is very minor. The resulting intercept age of Ke9 is 401 ± 3 Ma (Fig. 4), in agreement with a mean age of 406 ± 17 Ma for sample Ke9. And third, plotting all laser-spot matrix ages on a cumulative frequency probability diagram (Fig. 7), there is a single narrow peak at 400 Ma. Finally, the observations outlined below suggest that subsequent to pseudotachylite formation there has been no significant argon loss by diffusion. In consequence, the age of ~400 Ma is the formation age of the pseudotachylites and not a cooling age.

K–Ar biotite ages from western Kenya cluster at around 470 Ma (Key et al., 1989 and references therein) and indicate the time when the basement rocks cooled through ~300°C. During the late- and post-orogenic evolution of the Mozambique Belt, the tectonically thickened crust was isostatically uplifted and exhumed (Smith and Mosley, 1993), and the gneisses along the Elgeyo Escarpment continued to cool. Apatite fission track data indicate that the base of a Cretaceous partial annealing zone, i.e. the 110°C isotherm, is at an elevation of 2.1 km at the northern

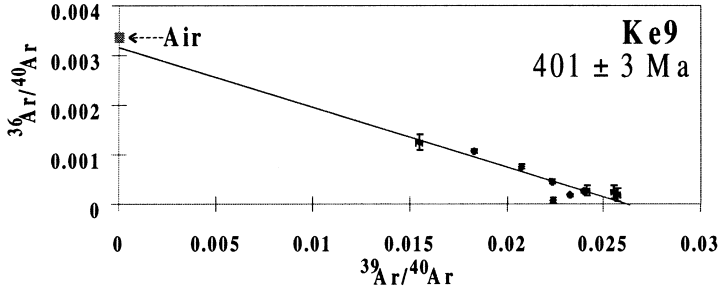

Fig. 4. Inverse isochron correlation diagram for laser spot data from pseudotachylite matrix from sample Ke9, with an intercept age of 401 ± 3 Ma.

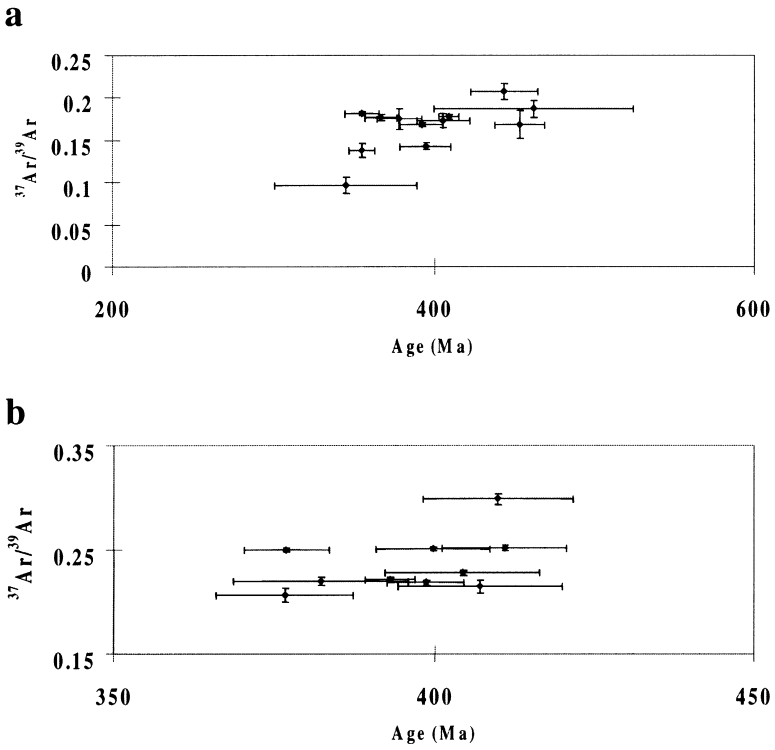

Fig. 5. $^{37}Ar/^{39}Ar$ ratios versus apparent ages plotted for matrix pseudotachylite laser spots. (a) Sample Ke4. (b) Sample P37 (see text for discussion).

Elgeyo Escarpment (Foster and Gleadow, 1996). This suggests that the pseudotachylites, sampled at an altitude of 1.7 km, were located 0.4 km below the base of the apatite partial annealing zone during the Late Palaeozoic/Mesozoic. Thus the host rock of the TFZ pseudotachylite was at a temperature of about 150°C when the pseudotachylites formed. Cooling of the basement and the pseudotachylytes to <60°C occurred during the Late Cretaceous, and

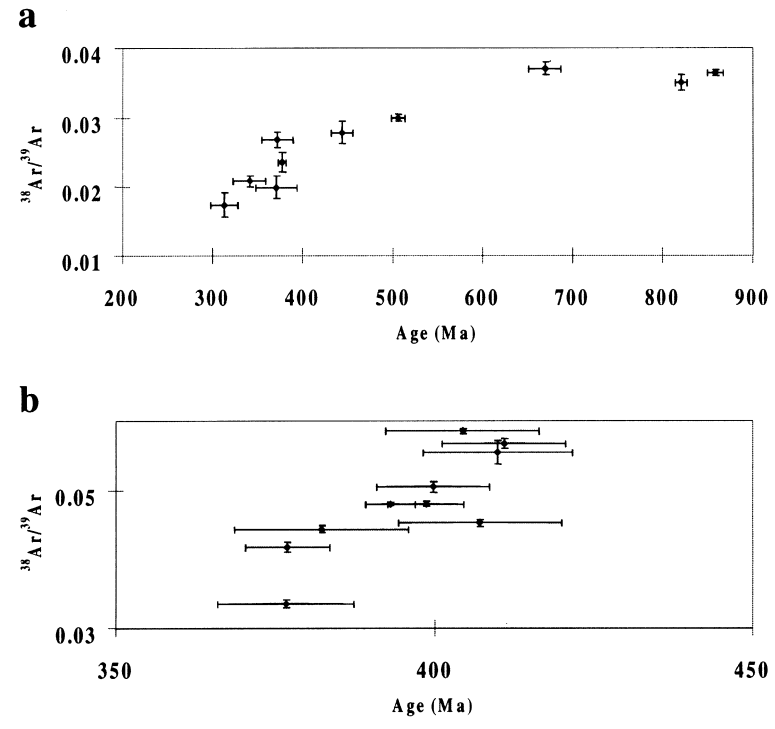

Fig. 6. $^{38}Ar/^{39}Ar$ ratios versus apparent ages plotted for matrix pseudotachylite laser spots. (a) Sample Ke1. (b) Sample P37 (see text for discussion).

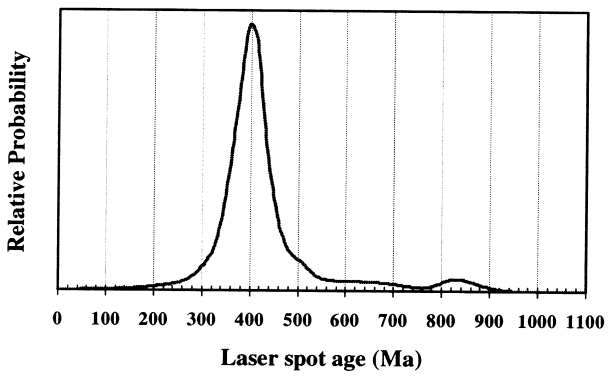

Fig. 7. Cumulative frequency plot of all laser spot ages from the five Tambach Fault Zone samples; a well defined peak at 400 Ma is interpreted as the formation age of the pseudotachylites.

final exhumation took place during the Tertiary formation of the northern Kenya Rift in the footwall of the Elgeyo normal fault.

7.2. Role of quartz and feldspar clasts and alteration products

Sample Ke1 has the widest matrix age range—313 ± 15 Ma to 858 ± 9 Ma—and the highest mean age (507 ± 192 Ma, Table 2). The oldest ages within sample Ke1, 669 ± 18 and 858 ± 9 Ma, correspond to analyses with the highest Cl/K ratios (Fig. 6a). This is regarded as a likely result of mixing of pseudotachylite matrix with quartz clasts containing fluid inclusions rich in Cl (e.g., Kelley et al. 1986; Cumbest et al. 1994), or of the influence of very fine-grained fragments of precursor rock biotite, or biotite microlites (biotite being another common source of chlorine). In the case of the TFZ pseudotachylites, it is more likely that high Cl/K ratios are due to analysing fine-grained quartz clasts, as electron microprobe investigations (Hetzel et al., 1996) found no evidence for either precursor rock biotite or biotite microlites in the matrix.

In sample Ke4, the oldest ages correspond to the highest Ca/K ratios (Fig. 5a), indicating mixing between pseudotachylite matrix material and feldspar clasts derived from the host-rock, which did not outgas during melt generation and rapid crystallisation. Nevertheless, the experimental results for sample Ke4 are relatively homogeneous, with a high proportion of ages within error of the 400 Ma age for pseudotachylite formation (Table 2), and an average age of 397 ± 20 Ma. Sample P37 has an average laser-spot age of 396 ± 10 Ma and a total gas age of 405 ± 8 Ma (Table 2). Laser spot ages range from 377 ± 7 Ma to 411 ± 10 Ma (Table 1), with the oldest ages generally corresponding to the highest $^{37}Ar/^{39}Ar$ ratios (Fig. 5b) and $^{38}Ar/^{39}Ar$ ratios (Fig. 6b). This is indicative of contamination by chlorine-rich fluid inclusions in quartz and high-Ca feldspar clasts, respectively. Individual steps from the incremental-heating spectrum range from 260 ± 6 Ma to 471 ± 10 Ma (Fig. 3). Due to the disturbance of the argon system that is clear from the apparent age spectrum, and which is thought to result from excess argon contamination or from chlorine and calcium interference, the spectrum does not yield a plateau age. The lowest age from a single step is 260 ± 6 Ma, which is from the first step and is most likely the result of argon release from ultra-fine-grained feldspars in the matrix. With respect to the ages of steps two to six, which are 455 ± 10 Ma, 471 ± 10 Ma, 457 ± 9 Ma, 438 ± 9 Ma and 426 ± 9 Ma, respectively, the highest age corresponds to the second highest $^{38}Ar/^{39}Ar$ ratio, which is probably derived from chlorine-rich fluid inclusions in quartz. The highest temperature step did not yield the oldest age, but corresponds to both the highest Ca/K ratio and the highest Cl/K ratio, the likely result of argon outgassing from high-Ca feldspar clasts and chlorine-rich fluid inclusions in quartz. The total gas age for the incrementally-heated sample P37 is within error of the mean age of all laser spots for this sample. However, the release spectrum indicates that the total gas age comprises argon from the pseudotachylite matrix in addition to possible alteration products and both quartz and feldspar clasts. The total gas age, therefore, probably reflects an average of all sources of argon, rather than the age of pseudotachylite formation. It is either coincidence that this average is within error of the laser spot ages due to the overwhelming influence of the pseudotachylite matrix over the alteration products and feldspar-derived argon, or the spatial resolution of the laser is still too low to resolve the differences between each argon source.

7.3. Tectonic implications of the $^{40}Ar/^{39}Ar$ dating

The late-stage tectonic evolution of the Mozambique Belt orogeny in Kenya was characterised by the formation of NW–SE-trending strike-slip faults, which have been interpreted to have formed between 530 and 430 Ma (Charsley, 1987; Key et al., 1989; Smith and Mosley, 1993). The $^{40}Ar/^{39}Ar$ formation age of ~400 Ma for the pseudotachylites in the TFZ is thus in general agreement with the understanding of the geological history of the Mozambique Belt. However, it indicates that the tectonic activity within the Mozambique Belt continued past 430 Ma, and the pseudotachylite-generating strike-slip faults formed as late as 400 Ma.

Smith and Mosley (1993) suggested that seismic slip on the Elgeyo normal fault during Cenozoic rifting has been accommodated by movements along NW–SE-oriented basement structures, which in turn may have generated the pseudotachylites. This hypothesis can be clearly rejected on the basis of the new $^{40}Ar/^{39}Ar$ ages presented here, and although the inherited basement structures may have been locally reactivated as transfer faults that link different normal fault segments, a reactivation beyond the rift margin is not supported by our data. This conclusion is supported by the observation that the Miocene Basin Gishu Phonolites and the underlying Tambach sediments are not affected by

faulting (Hetzel and Strecker, 1994). Due to the erosional retreat of the Elgeyo Escarpment, the reactivated portions of the old strike-slip faults can, unfortunately, not be studied in the field.

8. Conclusions

If bulk sampling techniques such as incremental-heating are applied to samples containing significant proportions of either quartz or feldspar or both, inherited ^{40}Ar and ^{38}Ar derived from fluid inclusions in quartz and/or inherited ^{40}Ar and ^{37}Ar derived from feldspar, may result in the disturbance of the spectra due to contamination. The $^{40}Ar/^{39}Ar$ laser-probe technique has a spatial resolution of approximately 50 μm, and may avoid all but the finest-grained host-rock porphyroclasts and microlites, greatly reducing the likelihood of contamination by these additional argon components. A further advantage of the in situ laser-probe argon extraction technique is that if it is impossible to select a sample with no alteration, it remains possible to analyse the few unaltered regions with pristine pseudotachylite, if present, down to a size of approximately 50 μm.

Our results demonstrate that the laser probe $^{40}Ar/^{39}Ar$ technique is a powerful tool that can be used to determine the age of pseudotachylite-bearing brittle faults in the upper crust, for which there is currently no other routine method to obtain any direct age information. Using the bulk incremental-heating technique is less effective and may result in 'mixed ages' from the isotopic contributions of precursor-rock clasts, inherited argon, radiogenic argon from the matrix, alteration products, and excess argon. Further improvement of the analytical capabilities of mass spectrometers and an increasing spatial resolution of lasers, will enable the analysis of ever smaller volumes of material, and the extraction of more detailed geochronological information. In the near future this may help to constrain the age of brittle fault rocks more precisely than is possible at present.

Acknowledgements

Simon Kelley is gratefully acknowledged for both technical advice and the use of the infrared laser extraction system at The Open University, UK. Uwe Reimold is thanked for two most constructive reviews of this manuscript, and an anonymous reviewer is acknowledged for a brief review of an early version. SS was financially supported by NERC studentship GT4/95/243/E followed by Research Council of Norway (NFR) grant 131817/431. RH was financially supported by the Deutsche Forschungsgemeinschaft (D.F.G.).

References

Arnaud, N.O., Kelley, S.P., 1995. Evidence for excess argon during high-pressure metamorphism in the Dora Maira Massif (western Alps, Italy), using an ultra-violet laser ablation microprobe $^{40}Ar/^{39}Ar$ technique. Contributions to Mineralogy and Petrology 121, 1–11.

Berger, G.W., York, D., 1981. Geothermometry from $^{40}Ar/^{39}Ar$ dating experiments. Geochimica et Cosmochimica Acta 45, 39–44.

Bossière, G., 1991. Petrology of pseudotachylites from the Alpine fault of New Zealand. Tectonophysics 196, 173–193.

Burke, K., Sengör, A.M.C., 1986. Tectonic escape in the evolution of the continental crust. In: Barazangi, M., Brown, L. (Eds.), Reflection Seismology: The Continental Crust. American Geophysical Union Geodynamics Series, 14, pp. 41–53.

Carroll, M.R., Stolper, E.M., 1993. Argon solubility in silicate melts and glasses: New experimental results for argon and the relationship between solubility and ionic porosity. Geochimica et Cosmochima Acta 57, 5039–5051.

Charsley, T.J., 1987. Geology of the Laisamis area. Geological Survey of Kenya Report, p. 106.

Cumbest, R.J., Johnson, E.L., Onstott, T.C., 1994. Argon composition of metamorphic fluids: implications for $^{40}Ar/^{39}Ar$ geochemistry. Geological Society of America Bulletin 106, 942–951.

Dalrymple, G.B., Lanphere, M.A., 1974. $^{40}Ar/^{39}Ar$ age spectra of some undisturbed terrestrial samples. Geochimica et Cosmochimica Acta 38, 715–738.

Draper, D.S., Carroll, M.R., 1995. Argon diffusion and solubility in silicic glasses exposed to an Ar–He gas mixture. Earth and Planetary Science Letters 132, 15–24.

Dunlap, W.J., Fossen, H., 1998. Early Paleozoic orogenic collapse, tectonic stability, and late Paleozoic continental rifting revealed through thermochronology of K-feldspars, Southern Norway. Tectonics 17, 604–620.

Eide, E..A., Torsvik, T.H., Andersen, T.B., 1997. Absolute dating of fault breccias: Late Palaeozoic and early Cretaceous fault reactivation in Western Norway. Terra Nova 9, 135–139.

Foster, D.A., Gleadow, A J.W., 1996. Structural framework and denudation history of the flanks of the Kenya and Anza Rifts, East Africa. Tectonics 15, 258–271.

Freeman, S.R., Inger, S., Butler, R.W.H., Cliff, R.A., 1997. Dating deformation using Rb-Sr in white mica: Greenschist facies deformation ages from the Entrelor Shear Zone, Italian Alps. Tectonics 16, 57–76.

Heizler, M.T., Harrison, T.M., 1988. Multiple-trapped argon isotope components revealed by $^{40}Ar/^{39}Ar$ isochron analysis. Geochimica et Cosmochimica Acta 52, 1295–1303.

Hetzel, R., Strecker, M.R., 1994. Late Mozambique Belt structures in western Kenya and their influence of the Cenozoic Kenya Rift. Journal of Structural Geology 16, 189–201.

Hetzel, R., Altenberger, U., Strecker, M.R., 1996. Structural and chemical evolution of pseudotachylites during seismic events. Mineralogy and Petrology 58, 33–50.

Inger, S., Ramsbotham, W., Cliff, R.A., Rex, D.C., 1996. Metamorphic evolution of the Sesia-Lanzo Zone, Western Alps: Time constraints from multi-system chronology. Contributions to Mineralogy and Petrology 126, 152–168.

Karson, J.A., Brooks, C.K., Storey, M., Pringle, M.S., 1998. Tertiary faulting and pseudotachylites in the East Greenland volcanic rifted margin: Seismogenic faulting during magmatic construction. Geology 26, 39–42.

Kelley, S.P., Turner, G., Butterfield, A.W., Shepherd, T.J., 1986. The source and significance of argon in fluid inclusions from areas of mineralization. Earth and Planetary Science Letters 79, 303–318.

Kelley, S.P., Reddy, S.M., Maddock, R., 1994. Laser-probe $^{40}Ar/^{39}Ar$ investigation of a pseudotachylite and its host rock from the Outer Isles Thrust, Scotland. Geology 22, 443–446.

Key, R.M., Charsley, T.J., Hackman, B.D., Wilkinson, A.F., Rundle, C.C., 1989. Superimposed Upper Proterozoic collision-controlled orogenies in the Mozambique Orogenic Belt of Kenya. Precambrian Research 44, 197–225.

Killick, A.M., Thwaites, A.M., Germs, G.J., 1988. Pseudotachylite

associated with a bedding-parallel fault zone between the Witwatersrand and Ventersdorp Supergroups, South Africa. Geologische Rundschau 77, 329–344.

Kralik, M., Klima, K., Riedmüller, G., 1987. Dating fault gouges. Nature 327, 315–317.

Lanphere, M., Dalrymple, G.B., 1978. The use of $^{40}Ar/^{39}Ar$ data in evaluation of disturbed K–Ar systems: United States Geological Survey Open-file Report 78-701, 241–243.

Lin, A., 1994. Glassy pseudotachylite veins from the Fuyun fault zone, northwest China. Journal of Structural Geology 16, 71–83.

Lippolt, H.J., Hess, J.C., 1988. HD-B1-biotite reference material for K-Ar chronometry. Abstract of the International Symposium FT Dating, Besançon, A5-6.

Maboko, M.A.H., Boelrijk, N.A.I.M., Priem, H.N.A., Verdurmen, A.E.Th., 1985. Zircon U-Pb and biotite Rb-Sr dating of the Wami River granulites, Eastern Granulites, Tanzania: Evidence for approximately 715 Ma old granulite-facies metamorphism and final Pan-African cooling approximately 475 Ma ago. Precambrian Research 30, 361–378.

Maddock, R.H., Grocott, J., Van Nes, M., 1987. Vesicles, amygdales and similar structures in fault-generated pseudotachylites. Lithos 20, 419–432.

Magloughlin, J.F., Spray, J.G., 1992. Frictional melting processes and products in geological materials: introduction and discussion. Tectonophysics 204, 197–204.

McConville, P., Kelley, S.P., Turner, G., 1989. Laserprobe $^{40}Ar/^{39}Ar$ studies of the Peace River shocked L6 chondrite. Geochimica et Cosmochima Acta 52, 2487–2499.

McNulty, B.A., 1995. Pseudotachylite generated in the semi-brittle and brittle regimes, Bench Canyon shear zone, central Sierra Nevada. Journal of Structural Geology 17, 1507–1521.

Mugisha, F., Ebinger, C.J., Strecker, M., Pope, D., 1997. Two-stage rifting in the Kenya rift: implications for half-graben models. Tectonophysics 278, 63–81.

Müller, W. 1997. Isotopic Dating of Deformation Using Microsampling Techniques: The Evolution of the Periadriatic Fault System (Alps). PhD Dissertation, ETH Zürich, Nr. 12580, pp. 132

Reddy, S.M., Kelley, S.P., Wheeler, J., 1996. A $^{40}Ar/^{39}Ar$ laser probe study of micas from the Sesia Zone, Italian Alps; implications for metamorphic and deformation histories. Journal of Metamorphic Geology 14, 493–508.

Reimold, W.U., Jessberger, E.K., Stephan, T., 1990. $^{40}Ar/^{39}Ar$ dating of pseudotachylite from the Vredefort Dome, South Africa: a progress report. Tectonophysics 171, 139–152.

Reimold, W.U., Stephan, T., Jessberger, E.K., 1992. Testing young ^{40}Ar-^{39}Ar ages for Vredefort pseudotachylites. South African Journal of Science 88, 563–573.

Reimold, W.U., 1995. Pseudotachylite in impact structures: generation by friction melting and shock brecciation? A review and discussion. Earth Science Reviews 39, 247–265.

Reimold, W.U., 1998. Exogenic and endogenic breccias: a discussion or major problematics. Earth Science Reviews 43, 25–47.

Reimold, W.U., Köberl, C., Fletcher, P., Killick, A.M., Wilson, J.D., 1999. Pseudotachylitic breccias from fault zones in the Witwatersrand Basin, South Africa: evidence of autometasomatism and post-brecciation alteration processes. Mineralogy and Petrology 66, 25–53.

Renne, P.R., Swisher, C.C., Deino, A.L., Karnet, D.B., Owens, T.L., DePaolo, D.J., 1998. Intercalibration of standards, absolute ages and uncertainties in $^{40}Ar/^{39}Ar$ dating. Chemical Geology (Isotope Geoscience) 145, 117–152.

Resor, P.G., Chamberlain, K.R., Frost, C.D., Snoke, A.W., Frost, B.R., 1996. Direct dating of deformation: U-Pb age of syndeformational sphene growth in the Proterozoic Laramie Peak shear zone. Geology 24, 623–626.

Ruffét, G., Gruau, G., Ballèvre, M., Féraud, G., Philippot, P., 1997. Rb-Sr and $^{40}Ar/^{39}Ar$ laser probe dating of high-pressure phengites from the Sesia Zone (Western Alps): underscoring of excess argon and new age constraints on the high-pressure metamorphism. Chemical Geology (Isotope Geoscience) 141, 1–18.

Scaillet, S., 1996. Excess ^{40}Ar transport scale and mechanism in high-pressure phengites; a case study from an eclogitized metabasite of the Dora-Maira nappe, Western Alps. Geochimica et Cosmochimica Acta 60, 1075–1090.

Schärer, U., Zhang, L.-S., Tapponier, P., 1994. Duration of strike-slip movements in large shear zones: The Red River belt, China. Earth and Planetary Science Letters 126, 379–397.

Shackleton, R.M., 1986. Precambrian collision tectonics in Africa. In: Coward, M.P., Ries, A.C. (Eds.). Collision Tectonics, Geological Society of London Special Publication 19, , pp. 329–349.

Sherlock, S.C., Arnaud, N.O., 1999. Flat plateau and impossible isochrons: apparent $^{40}Ar/^{39}Ar$ geochronology in a HP terrain. Geochimica et Cosmochimica Acta 63, 2835–2838.

Sherlock, S.C., Kelley, S.P., Inger, S., Harris, N.B.W., Okay, A.I., 1999. $^{40}Ar/^{39}Ar$ geochronology of high-pressure metamorphism and exhumation in the Tavsanli Zone, NW Turkey. Contributions to Mineralogy and Petrology 137, 46–58.

Shibata, T., Takahashi, E., Matsuda, J.I., 1998. Solubility of neon, krypton, and xenon in binary and ternary silicate systems: A new view on noble gas solubility. Geochimica et Cosmochimica Acta 62, 1241–1253.

Sibson, R.H., 1975. Generation of pseudotachylite by ancient seismic faulting. Geophysical Journal of the Royal Astronomic Society 43, 775–794.

Smith, M., Mosley, P., 1993. Crustal heterogeneity and basement influence on the development of the Kenya Rift, East Africa. Tectonics 12, 591–606.

Spray, J.G., 1992. A physical basis for the frictional melting of some rock-forming minerals. Tectonophysics 204, 205–221.

Spray, J.G., 1993. Viscosity determinations of some frictionally generated silicate melts: Implications for fault zone rheology at high strain zones. Journal of Geophysical Research 98, 8053–8068.

Spray, J.G., Kelley, S.P., Reimold, W.U., 1995. Laser-probe $^{40}Ar/^{39}Ar$ dating of coesite-bearing and stishovite-bearing pseudotachylites and the age of the Vredefort impact event. Meteoritics 30, 335–343.

Steiger, R.H., Jäger, E., 1977. Subcommission on geochronology: Convention on the use of decay constants in geo- and cosmochronology. Earth and Planetary Science Letters 36, 359–361.

Thompson, L.M., Spray, J.G., Kelley, S.P., 1998. Laser probe $^{40}Ar/^{39}Ar$ dating of a pseudotachylite from the Sudbury Structure: Evidence for postimpact thermal overprinting in the Northern Range. Meteoritics and Planetary Science 33, 1259–1269.

Trieloff, M., Reimold, U.W., Kunz, J., Boer, R.H., Jessberger, E.K., 1994. $^{40}Ar/^{39}Ar$ thermochronology of pseudotachylite at the Ventersdorp Contact Reef, Witwatersrand basin. South African Journal of Geology 97, 365–384.

White, B.S., Brearley, M., Montana, A., 1989. Solubility of argon in silicate liquids at high pressures. American Mineralogist 74, 513–529.